

Article

# Precipitation Hardening of the HVOF Sprayed Single-Phase High-Entropy Alloy CrFeCoNi

Martin Löbel <sup>1,\*</sup>, Thomas Lindner <sup>1</sup>, Ralph Hunger <sup>2</sup>, Robin Berger <sup>2</sup> and Thomas Lampke <sup>1</sup>

<sup>1</sup> Materials and Surface Engineering Group, Institute of Materials Science and Engineering, Chemnitz University of Technology, D-09107 Chemnitz, Germany; th.lindner@mb.tu-chemnitz.de (T.L.); thomas.lampke@mb.tu-chemnitz.de (T.L.)

<sup>2</sup> BorTec GmbH & Co. KG, D-50354 Hürth, Germany; r.hunger@bortec.de (R.H.); r.berger@bortec.de (R.B.)

\* Correspondence: martin.loebel@mb.tu-chemnitz.de

Received: 22 June 2020; Accepted: 17 July 2020; Published: 20 July 2020



**Abstract:** The application of high-entropy alloys (HEA) in surface technology has great potential due to the high corrosion and wear resistance. A further improvement can be achieved by applying thermochemical treatments. Powder-pack boriding enables the formation of a protective precipitation layer. This process has already been applied for cast HEAs causing the formation of a diffusion-enriched surface layer and a distinct increase in wear resistance. In the current investigations, the alloy CrFeCoNi with a single-phase face-centred cubic (fcc) structure is considered. An efficient application can be achieved by limiting the material usage of HEAs to the surface. Therefore, the high-velocity-oxygen-fuel (HVOF) thermal spray process is applied. Boriding was conducted with an adapted powder-pack routine. Furthermore, borided bulk HEAs were considered as a reference. The influence of the production route and boriding treatment on the microstructure, phase formation, and properties was investigated in detail. For the coating and the cast HEA, a precipitation layer is formed. Hence, the hardness and wear resistance are significantly increased. The current study proves the suitability of the investigated process combination.

**Keywords:** high-entropy alloy; HEA; coating; HVOF; boriding; precipitation; phase formation; microstructure; wear

## 1. Introduction

High-entropy alloys (HEA) are a new group of multiprincipal alloys comprised of at least four alloying elements. Early studies focused on alloys forming solid solutions with face-centred cubic (fcc) and body-centred cubic (bcc) structure [1,2]. Single-phase fcc alloys exhibit a high ductility but relatively low hardness and strength, whereas single-phase bcc alloys are characterised by a reduced ductility and increased strength [3].

To overcome the inherent disadvantages of fcc HEAs, several approaches have been considered. Thermochemical treatments are conducted to improve surface properties e.g., hardness, sliding characteristics, and wear resistance. These processes are state of the art for cast iron- and nickel-base alloys. One group of thermochemical treatments is interstitial hardening processes, which are conducted by nitriding, carburising, and nitrocarburising [4]. Only limited investigations have been conducted for HEAs. Previous investigations by Lindner et al. proved the suitability of a gasnitrocarburisation process for the treatment of the alloys Cr(Mn)FeCoNi. An increase of hardness and wear resistance could be achieved by the formation of an expanded austenitic phase, whereas the corrosion resistance was not significantly impaired [5]. Besides thermochemical treatment with gaseous media, an enrichment of the surface could also be achieved by plasma nitriding. Nishimoto et al. reported the successful plasma nitriding of the alloy CrMnFeCoNi, causing the formation of an expanded fcc phase [6]. Furthermore,

interstitial alloying through a powder metallurgical route as well as the dissolution of the interstitial elements carbon and nitrogen in the melt were reported in literature [7,8].

For iron- and nickel-base material, the highest hardness values can be achieved by the precipitation hardening process boriding. The formation of thermally stable borides enables applications at elevated temperatures. Powder-pack boriding is the most common variant used in industry [9]. Boriding of the fcc phase HEAs Cr(Mn)FeCoNi has been investigated by Lindner et al., proving the formation of a precipitation layer and a significant increase of hardness and wear resistance. In addition to borides, silicon-rich phases were formed as well due to interactions with the filler material SiC, which demonstrates the necessity of applying alternative processing routes [10]. Further investigations by Hou et al. proved the formation of a precipitation layer composed of (Ni,Co,Fe)<sub>2</sub>B and CrB for the fcc HEA Al<sub>0.25</sub>CoCrFeNi. A reduction of wear rate and the coefficient of friction (COF) could be achieved [11]. The formation of borides has also been proved for the alloy Al<sub>0.5</sub>CoCrCuFeNiB<sub>x</sub> derived from the liquid state [12].

So far, thermochemical treatments have focused on cast HEAs. However, due to the high content of expensive alloying elements, in particular cobalt, a reduction of material usage is required, which can be achieved by coating processes. Thermal spraying enables the processing of a wide range of substrates and coating materials [13]. The processing of HEAs by thermal spraying has also been reported in literature [14–16]. Dense coatings with a low degree of oxidation can be produced by high kinetic processes e.g., high-velocity-oxygen-fuel (HVOF) thermal spraying [17,18].

The successful process combination of thermal spraying and subsequent thermochemical treatment has already been proven for austenitic stainless coatings [19,20].

The current feasibility study investigates the process combination of HVOF thermal spraying the fcc HEA CrFeCoNi and thermochemical treatment by powder-pack boriding. To avoid the formation of silicon-rich phases, an adapted process routine is applied. A cast HEA of the same composition is borided as a reference. The formation of microstructure and phases in dependence of the production route is studied in detail. Furthermore, the influence on the wear resistance under various conditions is considered.

## 2. Materials and Methods

In the current investigations, cast HEAs and coatings were considered for a thermochemical treatment by boriding. Bulk samples of the equimolar alloy CrFeCoNi were produced by arc-melting. Elemental granules with a purity of  $\geq 99.9\%$  and a total weight of 10 g were balanced and mixed. The melting process was conducted in a water-cooled copper crucible using a tungsten electrode to ignite the arc. The furnace chamber was evacuated to a pressure of  $2 \times 10^{-4}$  mbar and filled with argon prior to the melting process. The production of homogeneous samples was ensured by performing three melting steps, with the samples being flipped after each step. Subsequently, the as-cast samples were cut in slices with a thickness of 1.5 mm with an Accutom 50 (Struers, Willich, Germany).

The feedstock powder for the thermal spray process was produced by inert gas atomisation. For the coating process, stainless-steel substrates (EN 1.4404) were prepared by corundum blasting using Alodur EK F 24 blasting media with a particle size in the range of 600 to 850  $\mu\text{m}$ . All substrates were roughened with a pressure of 2.5 bar under an angle of  $70^\circ$ , resulting in roughness values of  $R_a$ : 5.4  $\mu\text{m}$  and  $R_z$ : 37.8  $\mu\text{m}$ . Cleaning of the substrates was performed ultrasonically in an ethanol bath. For the coating process, the liquid-fuelled HVOF system K2 (GTV Verschleisschutz GmbH, Luckenbach, Germany) with the parameters summarised in Table 1 was applied.

**Table 1.** High-velocity-oxygen-fuel (HVOF) coating parameters of CrFeCoNi feedstock powder.

O <sub>2</sub> (L/min)	Kerosene (L/h)	$\lambda$	Ar (L/min)	Nozzle	Powder Feed Rate (g/min)	Spraying Distance (mm)	Relative Traverse Speed (m/s)	Spray Path Offset (mm)
810	22.5	1.1	2 × 11	100/12	2 × 40	360	1.0	5

Eight coating layers were deposited with intermediate cooling periods to achieve a final coating thickness of approximately 250  $\mu\text{m}$ . Prior to the thermochemical treatment, the surface was ground up to Grit 4000 (US#1200).

The thermochemical treatment of the bulk samples and coatings was conducted in a powder-pack process using an adapted process routine with the parameters summarised in Table 2.

**Table 2.** Powder-pack boriding parameters.

Boriding Agent	Temperature	Duration	Atmosphere
Ekabor <sup>®</sup> Ni	860 °C	5 h	Ar

A detailed characterisation of microstructure and phase formation has been conducted for bulk samples and coatings in both the untreated and borided state as well as for the feedstock powder. Metallographic cross-sections were prepared by standard metallographic procedures and investigated in the scanning electron microscope (SEM) LEO 1455VP (Zeiss, Jena, Germany). For the visualisation of material contrast, a backscattered electron detector (BSD) has been applied. The chemical composition was determined with the integrated energy-dispersive X-ray spectroscopy (EDS) system EDS GENESIS (EDAX, Mahwah, NJ, USA). The particle size distribution of the feedstock powder was determined by laser diffraction analyses using a Cilas 920 device (Cilas, Orléans, France). Depth profiles of the elemental concentration were determined for the borided samples by glow discharge spectroscopy (GDOS) using a GDA 750 spectrometer (Spectrums Analytik GmbH, Hof, Germany). For all measurements, a 2.5 mm anode, 800 V, 25 mA and 3 hPa argon pressure were applied. The sputtering rate was determined by conducting various measurements with a maximum measurement time of 600 s and an interval of 100 s. For the determination of the sputter depth, a 3D profilometer MikroCAD (LMI, Teltow, Germany) was used. For phase determination, measurements by X-ray diffraction (XRD) have been conducted with a D8 Discover diffractometer (Bruker AXS, Billerica, MA, USA) equipped with a 1D Lynxeye XE detector (Bruker AXS, Billerica, MA, USA). A diffraction angle range of 20° to 130° was investigated using Co K $\alpha$  radiation. The phase formation of castings and HVOF coatings in borided state was determined by measurements at the surface and with a surface distance of approximately 14  $\mu\text{m}$ . Therefore, the top layer was removed by GDOS.

Selective hardness measurements have been conducted by nanoindentation using the nanoindenter UNAT (ASMEC GmbH, Radeberg, Germany) with a Berkovich tip. A load of 10 mN has been applied for all indents. The average value and standard deviation were calculated from ten indents.

Furthermore, the wear behaviour was investigated under sliding, reciprocating, and abrasive wear conditions. For the investigation of the sliding wear behaviour in a ball-on-disk test, a Tetra basalt tester (Tetra, Ilmenau, Germany) has been applied. The wear test parameters were selected on the basis of ASTM G 99 [21]. The reciprocating wear behaviour was investigated in a Wazau SVT 40 device (Wazau, Berlin, Germany), with the parameters specified on the basis of ASTM G 133 [22]. The abrasive wear behaviour was investigated in a scratch test using a CSM Revetest-RST instrument (CSM Instruments SA, Peseux, Switzerland) with the parameters selected on the basis of ASTM G 171 [23]. The applied wear test parameters are summarised in Table 3.

**Table 3.** Wear test parameters.

Ball-On-Disk Test		Reciprocating Wear Test		Scratch Test	
Force	20 N	Force	26 N	Mode	progressive
Radius	5 mm	Frequency	40 Hz	Force	1–200 N
Speed	96 RPM	Time	900 s	Speed	2.5 mm/min
Cycles	15916	Amplitude	0.5 mm	Length	5 mm
Counter-body	Al <sub>2</sub> O <sub>3</sub> ( $\phi$ 6 mm)	Counter-body	Al <sub>2</sub> O <sub>3</sub> ( $\phi$ 10 mm)	Tip	truncated diamond cone ( $\phi$ 400 $\mu\text{m}$ )

Tactile measurements with a Hommel-Etamic T8000 device (Jenoptik, Villingen-Schwenningen, Germany) were conducted to evaluate the ball-on-disk test. The wear tracks of the reciprocating wear test were evaluated using the 3D profilometer described above. The remaining wear depth of the scratch test was determined by the CSM instrument. Therefore, a tactile measurement without load was conducted following the load cycle. For the calculation of the average value and standard deviation, three measurements have been considered for all wear tests. SEM investigations of the wear tracks were conducted to evaluate the underlying wear mechanisms.

### 3. Results and Discussion

#### 3.1. Feedstock Characterisation

The inert gas atomised feedstock powder of the alloy CrFeCoNi was characterised in detail. Cross-sections were prepared and investigated in SEM, Figure 1.

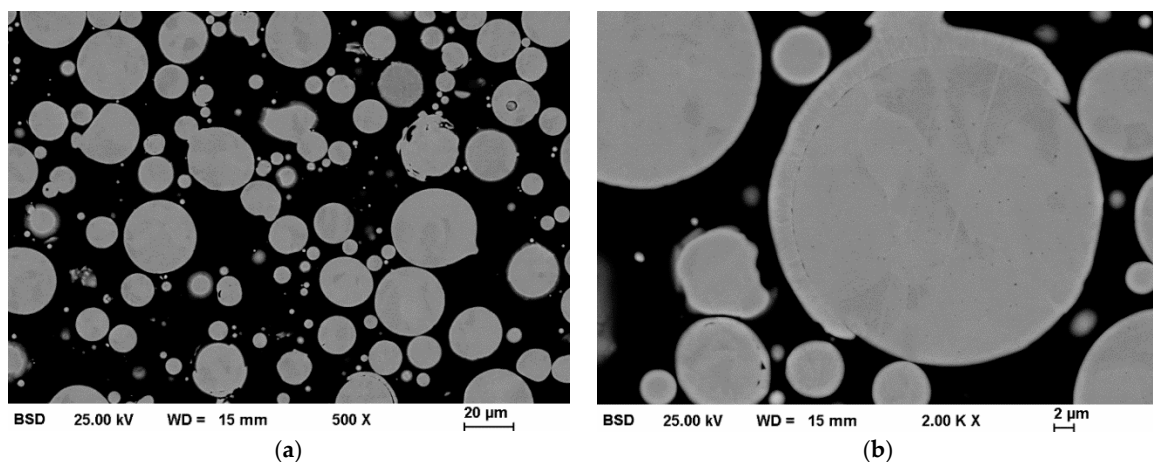


**Figure 1.** Scanning electron microscope (SEM) images (BSD) of inert gas atomised CrFeCoNi feedstock powder: (a) overview and (b) in detail.

Predominantly spherical powder particles are formed in the atomisation process. Additionally, a high content of particles with a diameter below 15 µm can be observed in the overview image. The particle size distribution was determined by laser diffraction analyses revealing a particle size range ( $-d_{90} + d_{10}$ ) of  $-28 + 8$  µm and a mean particle size ( $d_{50}$ ) of 20 µm. Furthermore, images with higher magnification reveal no distinct material contrast within single powder particles, showing that a homogeneous state has been formed.

#### 3.2. Chemical Composition

The chemical composition of the feedstock powder, the casting, and the coating in the untreated state was investigated by EDS. The results are summarised in Table 4.

**Table 4.** Chemical composition of atomised powder, casting, and HVOF coating in at.%, measured by energy-dispersive X-ray spectroscopy (EDS).

Sample	Cr	Fe	Co	Ni
atomised powder	25.7	25.0	24.6	24.7
casting	25.1	25.0	24.7	25.1
HVOF coating	25.1	25.4	24.7	24.9

The measured chemical composition of all states is in accordance with the nominal equimolar composition. Only minor deviations (<1 at.%) occur. Additionally, processing of the powder by means of HVOF thermal spraying causes no distinct change of the chemical composition.

The enrichment of boron in the surface layer after the thermochemical treatment by boriding was investigated by GDOS. In Figure 2, qualitative depth profiles of the casting and HVOF coating in borided state are shown.

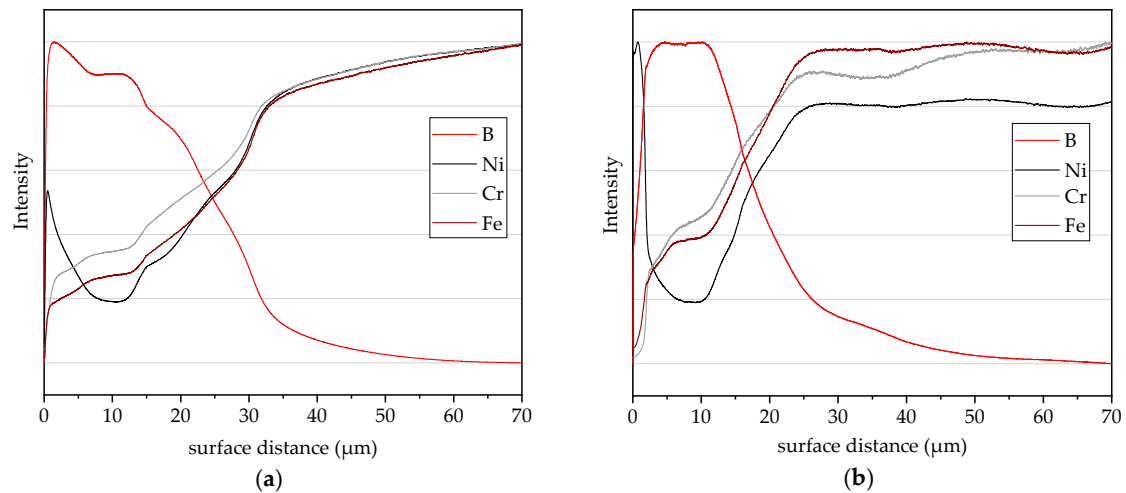


**Figure 2.** Qualitative depth profiles determined by glow discharge spectroscopy (GDOS): (a) cast CrFeCoNi in borided state; (b) borided HVOF coating CrFeCoNi.

The investigations by GDOS prove the successful enrichment with boron for the casting and coating. However, differences between the elemental depth profiles occur depending on the production route. For the casting, the boron concentration gradually decreases with increasing surface distance until it reaches a plateau at a depth of approximately 7 μm. For surface distances exceeding approximately 15 μm a distinct decrease of boron concentration occurs. A high concentration of nickel was determined at the surface. With increasing surface distance, a gradual decrease followed by a consistent concentration can be observed. The depth profiles of the elements nickel, chromium, and iron show a distinct increase in intensity starting at a surface distance of approximately 15 μm, where a strong decline of the boron concentration occurs.

For the HVOF coating, a constant boron intensity can be observed until a surface distance of approximately 11 μm. A high intensity of nickel was measured at the surface. The alloying elements nickel, chromium, and iron show profiles which are similar to the casting. However, fluctuations occur, which can be caused by the formation of a heterogeneous state comprising oxide lamellae and porosity.

### 3.3. Microstructure and Phase Formation

The microstructure of the borided samples was investigated in SEM (BSD) to visualise material contrast. Representative microstructural images are shown in Figure 3. A distinct material contrast occurs for both production routes. The cast CrFeCoNi in borided state exhibits a uniform dark layer at the surface. The low intensity of backscattered electrons indicates a low concentration of elements with a high atomic number and hence the formation of a diffusion-enriched surface layer with a thickness of approximately 10 μm. These results are in accordance with GDOS investigations. Beneath the boron-rich layer, a uniform second layer is formed. GDOS investigations reveal a reduced boron concentration in comparison to the outer boron-rich layer. The underlying base material shows no material contrast. Despite the conducted heat treatment during the boriding process, the homogeneous state of the equimolar alloy CrFeCoNi is preserved.

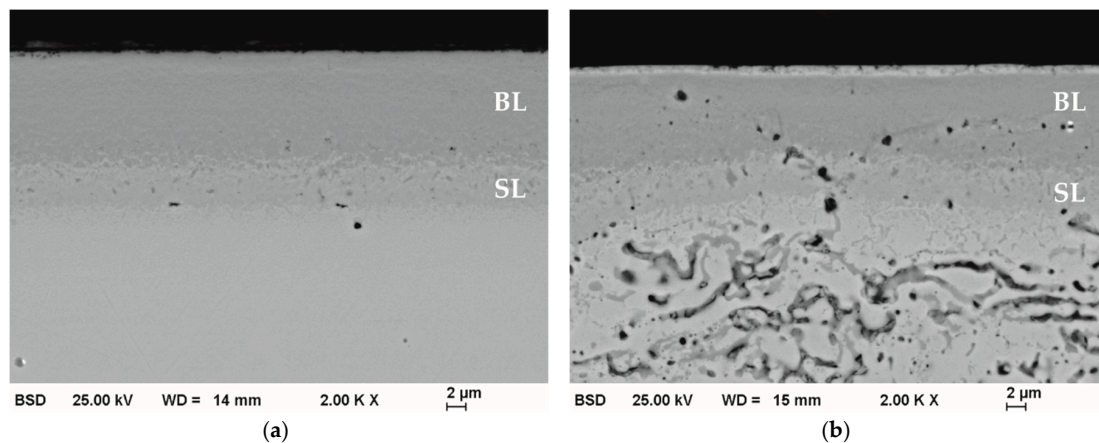


**Figure 3.** SEM images (BSD) of the borided surface layer comprising the B-rich layer (BL) and the second layer (SL): (a) cast CrFeCoNi; (b) HVOF coating CrFeCoNi.

For the CrFeCoNi HVOF coating, the formation of a diffusion-enriched surface layer with uniform thickness can be achieved. Small pores inherent to the coating in as-sprayed condition can also be observed after the thermochemical treatment. However, no single spray particles can be distinguished in the surface layer, showing that a homogenisation occurred. Beneath the boron-rich layer, a second enriched layer is formed in accordance to investigations on the casting. The underlying coating shows a dissolution of the coating structure. No clear delimitation with the second layer exists.

The phase formation in dependence of the production route and treatment condition was investigated by XRD. The resulting diffractograms are shown in Figure 4.

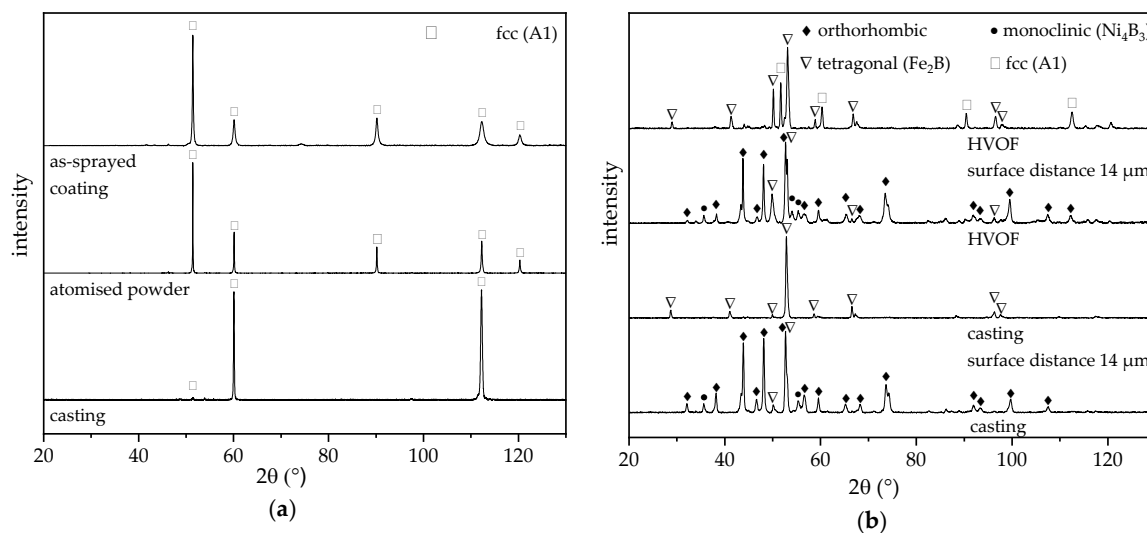


**Figure 4.** Diffractograms of CrFeCoNi: (a) feedstock powder, casting, and HVOF coating in untreated state; (b) casting and HVOF coating in borided state.

The diffractogram of the as-cast HEA solely exhibits diffraction peaks of an fcc phase with A1 structure ( $a = 3.57 \text{ \AA}$ ). However, not all related diffraction peaks occur, indicating a strong texture caused by the arc-melting process. The formation of a single-phase fcc structure without texture could be proven for the powder produced by inert gas atomisation. Processing by HVOF thermal spraying causes no phase transformation. The lattice parameter is not affected by the production route.

The phase formation of the casting and coating in borided state was investigated at the surface. Furthermore, XRD measurements were conducted with a surface distance of  $14 \text{ \mu m}$  to investigate the phase formation in the second layer. No diffraction peaks of the fcc phase with A1 structure appear for

the measurements conducted at the surface, showing that the diffusion enrichment with boron causes phase transformation.

For the casting a multiphase state is formed at the surface after the thermochemical treatment. The main diffraction peaks can be assigned to an orthorhombic phase ( $a = 5.43 \text{ \AA}$ ;  $b = 2.99 \text{ \AA}$ ;  $c = 4.02 \text{ \AA}$ ), which could not be assigned to known precipitation phases. The precipitation  $\text{Ni}_3\text{B}$  formed for nickel-base alloys also exhibits an orthorhombic lattice, however the lattice parameters are changed [24]. Furthermore, additional diffraction peaks of a tetragonal and monoclinic phase occur. These peaks can be assigned to  $\text{Fe}_2\text{B}$  and  $\text{Ni}_4\text{B}_3$ . Additional maxima with low intensity indicate the presence of additional minor phases. The investigation of the phase formation in the second layer reveals the formation of mainly  $\text{Fe}_2\text{B}$ . No diffraction peaks of  $\text{Ni}_4\text{B}_3$  and the orthorhombic phase are present.

No distinct deviation of the phase formation occurs for the borided HVOF coating in comparison to the casting at the surface. Besides a major orthorhombic phase,  $\text{Fe}_2\text{B}$  and  $\text{Ni}_4\text{B}_3$  are formed. The investigation of the phase formation in the second layer of the borided HVOF coating mainly revealed the formation of  $\text{Fe}_2\text{B}$ . However, diffraction peaks of the fcc phase with A1 structure occur as well. Microstructural investigations revealed no clear delimitation between the second layer and the unaffected coating.

In contrast to previous investigations by Lindner et al., no silicon-rich phases were formed due to the application of an adapted process routine [10].

### 3.4. Microhardness and Wear Behaviour

The influence of the microstructure and phase formation on the microhardness was investigated. The measured values are summarised in Table 5.

**Table 5.** Microhardness HV0.001 of CrFeCoNi casting and HVOF coatings in borided state.

Area	Casting	HVOF Coating
B-rich layer	2026 ± 82	1973 ± 86
second layer	1754 ± 164	1641 ± 134
unaffected material	270 ± 13	306 ± 30

The hardness values are strongly influenced by the thermochemical treatment. In comparison to the unaffected material, the hardness in the B-rich layer is clearly increased due to the formation of precipitates. Only a minor decrease of the hardness was observed in the second layer in comparison to the B-rich layer. However, the highest standard deviation was determined for this area. The hardness of the B-rich layer and the second layer is not significantly influenced by the production route. The hardness of the unaffected material is slightly increased for the HVOF coating. Due to the high cooling speed in the atomisation process and the incomplete melting in the HVOF coating process, the grain size is reduced in comparison to the casting, causing an increase in hardness.

Furthermore, the influence of the production route and boriding treatment on the wear behaviour under various conditions was investigated in detail. The results of the ball-on-disk, reciprocating wear, and scratch test are summarised in Figure 5.

The wear behaviour under sliding wear conditions in the ball-on-disk test is significantly influenced by the production route and the thermochemical treatment. The highest wear depth and hence lowest wear resistance was determined for the as-cast alloy. A reduced wear depth occurs for the CrFeCoNi coatings produced by HVOF. Phase analyses revealed no phase transformation in comparison to the as-cast alloy. Structural defects, e.g., pores and oxides, are formed for the coatings, but the hardness is slightly increased in comparison to the as-cast alloy. However, an increase of standard deviation occurs, due to the formation of a more heterogeneous state. Boriding of CrFeCoNi causes a distinct increase of wear resistance, whereas the lowest wear depth and area was determined for the casting. Only a minor deterioration occurs for the coating. The measured wear depths are below the determined thickness of the enriched surface layer, showing that no failure occurred.

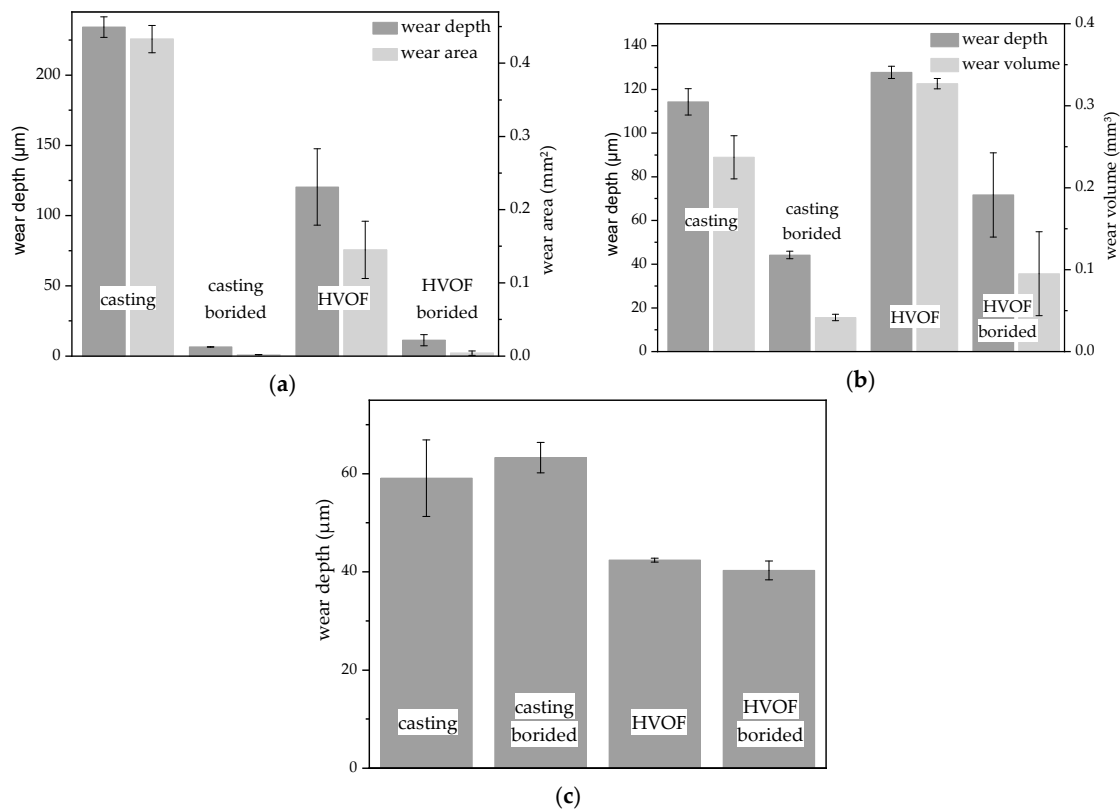


**Figure 5.** Results of wear investigations of CrFeCoNi casting and HVOF coating in untreated and borided state: (a) ball-on-disk test; (b) reciprocating wear test; and (c) scratch test.

The CrFeCoNi casting and coating reveal a similar wear resistance under reciprocating wear conditions. Thermochemical treatment by boriding causes a reduction of wear depth and area. However, a less pronounced improvement occurs in comparison to the investigations under sliding wear conditions in a ball-on-disk test. For both production routes, the measured wear depths exceeds the thickness of the diffusion-enriched surface layer. Hence, failure occurred under the applied test load. Previous wear investigations of the borided alloy Cr(Mn)FeCoNi under reciprocating conditions also revealed failure of the precipitation layer. Predominantly abrasive wear occurred [10]. The borided CrFeCoNi coatings exhibit an increased wear depth. This behaviour might be caused by the presence of structural defects, e.g., porosity and oxides. Furthermore, a distinct increase of standard deviation occurs in comparison to the casting.

The wear behaviour under abrasive conditions was investigated in a progressive mode scratch test. No significant influence of the thermochemical treatment on the wear depth of the casting was observed. Processing of the alloy CrFeCoNi by gas atomisation and HVOF thermal spraying causes an increase of wear resistance. The hardness of the coating is slightly increased in comparison to the casting. Thermochemical treatment of the coatings by boriding does not significantly influence the wear behaviour under abrasive conditions. For all investigated states no distinct spallation occurs, showing that the ductility can be preserved.

Due to the strong influence of the production route and thermochemical treatment on the wear behaviour under sliding and reciprocating conditions, the wear tracks were investigated by SEM. Representative images of the wear tracks of the ball-on-disk test are shown in Figure 6.

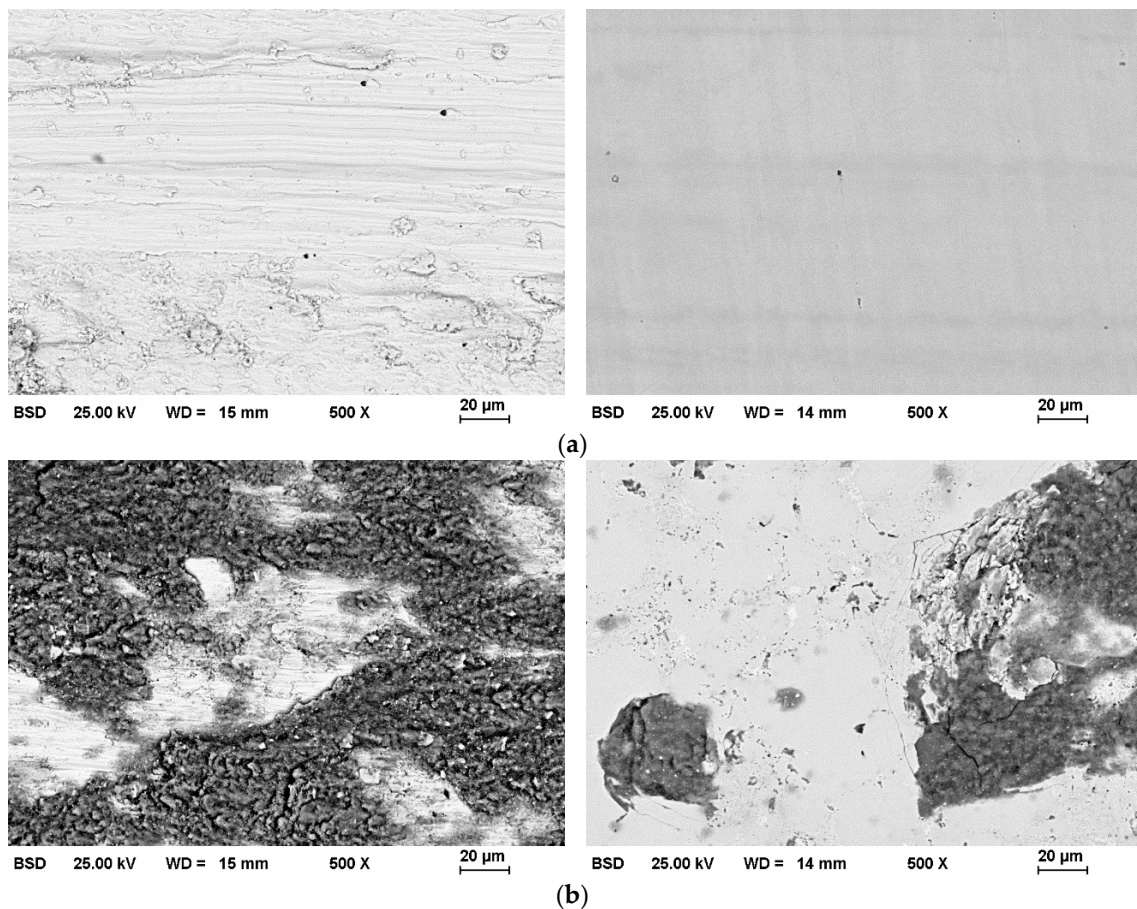


**Figure 6.** SEM images (BSD) of CrFeCoNi surface in untreated (left) and borided (right) state after ball-on-disk test: (a) casting and (b) HVOF coating.

The wear tracks of the untreated casting exhibit a relatively rough surface with grooves in wear direction. This indicates the presence of predominantly abrasive wear caused by the hard alumina counter body. In contrast, a smooth wear track occurs for the borided casting, showing that a protection of the material by the formation of the precipitation layer occurred. Only minor material removal was determined by tactile measurements. The wear track of the coating in untreated state shows a strong material contrast. The bright appearing areas can be assigned to the metallic coating, whereas the dark areas can be assigned to oxides. A rough surface of the oxides indicates that no stable protective oxide layer was formed. The borided coatings show a changed behaviour. Partially, a smooth surface similar to the casting occurs, proving a successful protection of the underlying material. However, local spallation and the formation of oxides can be observed.

Representative images of the surface after reciprocating wear test are shown in Figure 7.

For the untreated casting a distinct material contrast can be observed, indicating the formation of oxides. The rough surface shows that no stable protective oxide layer was formed. In the bright areas of the metallic material, grooves in wear direction occur due to abrasive wear. The wear track of the casting in borided state shows no distinct changes. The evaluation of wear depth shows that the investigated area is within the unaffected material. For the HVOF coating in untreated and borided state a similar appearance of the wear tracks with traces of abrasive wear and distinct oxide formation can be observed.

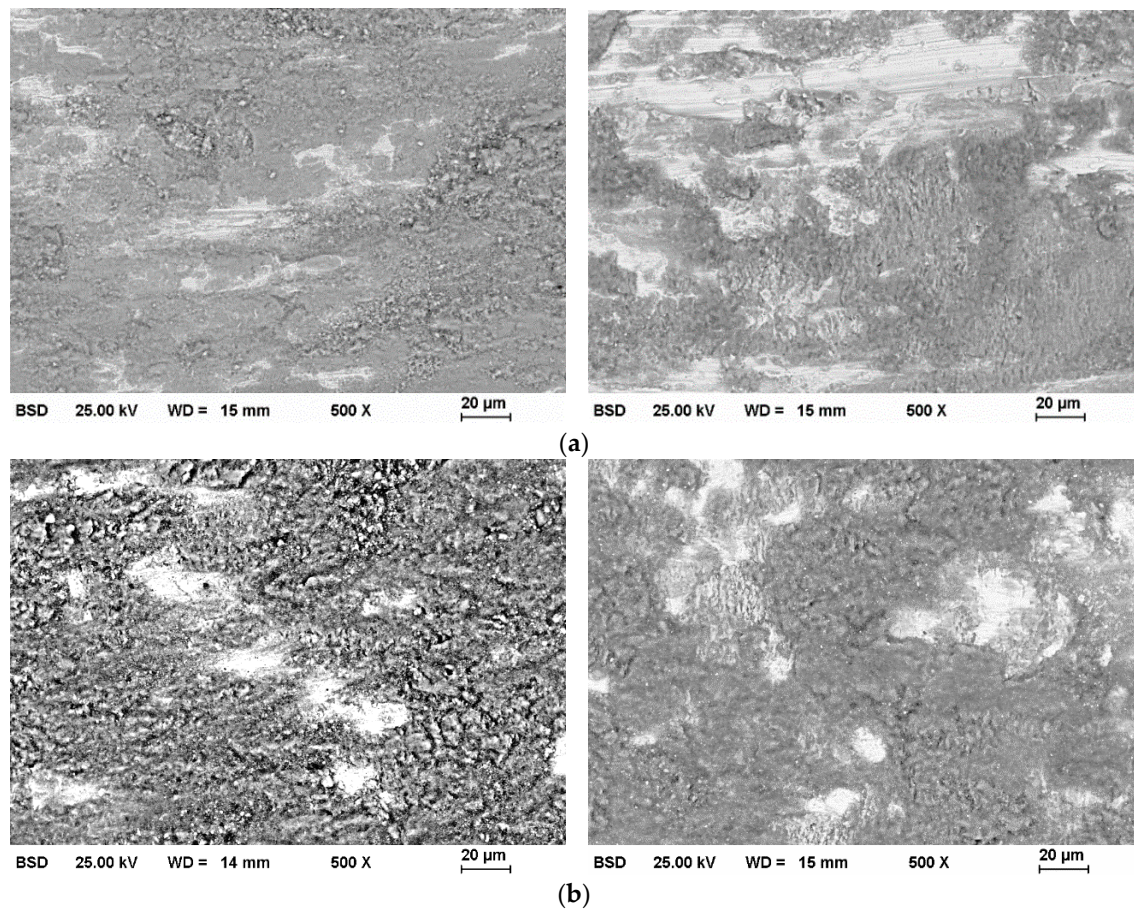


**Figure 7.** SEM images (BSD) of CrFeCoNi surface in untreated (left) and borided (right) state after reciprocating wear test: (a) casting and (b) HVOF coating.

#### 4. Summary and Conclusions

The process combination of depositing HEAs by thermal spraying and subsequent precipitation hardening was successfully conducted. Feedstock of the single-phase fcc HEA CrFeCoNi was produced by inert gas atomisation and processed by HVOF thermal spraying. Cast HEAs of the same composition were considered as a reference. The precipitation hardening was conducted by powder-pack boriding using an adapted process routine to avoid the formation of silicon-rich phases.

The formation of a precipitation layer could be achieved for the casting and coating. Phase analyses revealed the formation of an orthogonal phase,  $\text{Fe}_2\text{B}$  and  $\text{Ni}_4\text{B}_3$ . Furthermore, a second layer mainly comprised of  $\text{Fe}_2\text{B}$  was formed. No significant influence of the production route on the phase formation was observed. Thermochemical treatment of the HVOF coatings causes a homogenisation of the surface layer.

A significant increase of hardness could be achieved in the surface layer due the formation of precipitates. The wear behaviour could be improved especially under sliding wear conditions in ball-on-disk test. Additionally, under reciprocating wear conditions, the wear behaviour could be improved in comparison to the untreated state. However, failure of the surface layer occurred. The thermochemical treatment showed no distinct influence on the wear behaviour under abrasive wear conditions in scratch test. Due to structural defects, e.g., porosity and oxides, the wear resistance of castings in borided state could not be achieved for the borided coatings.

For the reduction of structural defects, a solution annealing step can be conducted before the thermochemical treatment. Furthermore, the thermochemical treatment of single-phase HEAs with a bcc structure is a promising alternative, enabling a higher hardness and strength of the base material.

**Author Contributions:** M.L. and T.L. (Thomas Lindner) conceived and designed the experiments. M.L., T.L. (Thomas Lindner), R.H., and R.B. performed the experiments, analysed the data, and wrote the paper. T.L. (Thomas Lampke) directed the research and contributed to the discussions and interpretations of the results. All authors have read and agreed to the published version of the manuscript.

**Funding:** This research was funded by the German Research Foundation (Deutsche Forschungsgemeinschaft/DFG), Grant No. La-1274/54-1 as well as by Sächsische Aufbaubank—Förderbank/SAB-100382175 by the European Social Fund ESF and the Free State of Saxony.

**Acknowledgments:** The authors thank Paul Seidel, Christian Loos and Steffen Clauß for metallographic preparation and investigation; Marc Pügner for conducting the XRD measurements; Elke Benedix for nanoindentation tests.

**Conflicts of Interest:** The authors declare no conflict of interest.

## References

1. Gao, M.C.; Yeh, J.-W.; Liaw, P.K.; Zhang, Y. *High-Entropy Alloys: Fundamentals and Applications*, 1st ed.; Springer International Publishing: Cham, Switzerland, 2016.
2. Manzoni, A.M.; Glatzel, U. New multiphase compositionally complex alloys driven by the high entropy alloy approach. *Mater. Charact.* **2018**, *147*, 512–532. [[CrossRef](#)]
3. Zhang, Y.; Zuo, T.T.; Tang, Z.; Gao, M.C.; Dahmen, K.A.; Liaw, P.K.; Lu, Z.P. Microstructures and properties of high-entropy alloys. *Prog. Mater. Sci.* **2014**, *61*, 1–93. [[CrossRef](#)]
4. Davis, J.R. *Surface Hardening of Steels: Understanding the Basics*; ASM International: Materials Park, OH, USA, 2002.
5. Lindner, T.; Löbel, M.; Saborowski, E.; Rymer, L.-M.; Lampke, T. Wear and corrosion behaviour of supersaturated surface layers in the high-entropy alloy systems CrMnFeCoNi and CrFeCoNi. *Crystals* **2020**, *10*, 110. [[CrossRef](#)]
6. Nishimoto, A.; Fukube, T.; Maruyama, T. Microstructural, mechanical, and corrosion properties of plasma-nitrided CoCrFeMnNi high-entropy alloys. *Surf. Coat. Technol.* **2019**, *376*, 52–58. [[CrossRef](#)]
7. Moravcik, I.; Cizek, J.; Gouvea, L.A.; Cupera, J.; Guban, I.; Dlouhy, I. Nitrogen interstitial alloying of CoCrFeMnNi high entropy alloy through reactive powder milling. *Entropy* **2019**, *21*, 363. [[CrossRef](#)]
8. Baker, I. Interstitials in f.c.c. high entropy alloys. *Metals* **2020**, *10*, 695. [[CrossRef](#)]
9. Kulka, M. *Current Trends in Boriding Techniques*; Springer Nature Switzerland AG: Cham, Switzerland, 2019.
10. Lindner, T.; Löbel, M.; Sattler, B.; Lampke, T. Surface hardening of FCC phase high-entropy alloy system by powder-pack boriding. *Surf. Coat. Technol.* **2019**, *371*, 389–394. [[CrossRef](#)]
11. Hou, J.; Zhang, M.; Yang, H.; Qiao, J.; Wu, Y. Surface strengthening in Al<sub>0.25</sub>CoCrFeNi high-entropy alloy by boronizing. *Mater. Lett.* **2019**, *238*, 258–260. [[CrossRef](#)]
12. Xiaotao, L.; Wenbin, L.; Lijuan, M.; Jinling, L.; Jing, L.; Jianzhong, C. Effect of boron on the microstructure, phase assemblage and wear properties of Al<sub>0.5</sub>CoCrCuFeNi high-entropy alloy. *Rare Metal. Mat. Eng.* **2016**, *45*, 2201–2207. [[CrossRef](#)]
13. Tucker, R.C. *ASM Handbook, Volume 5A: Thermal Spray Technology*; ASM International: Materials Park, OH, USA, 2013.
14. Li, J.; Huang, Y.; Meng, X.; Xie, Y. A review on high entropy alloys coatings: Fabrication processes and property assessment. *Adv. Eng. Mater.* **2019**, *21*, 1900343. [[CrossRef](#)]
15. Srivastava, M.; Jadhav, M.; Chakradhar, R.P.S.; Muniprakash, M.; Singh, S. Synthesis and properties of high velocity oxy-fuel sprayed FeCoCrNi<sub>2</sub>Al high entropy alloy coating. *Surf. Coat. Technol.* **2019**, *378*, 124950. [[CrossRef](#)]
16. Yan, X.H.; Li, J.S.; Zhang, W.R.; Zhang, Y. A brief review of high-entropy films. *Mater. Chem. Phys.* **2018**, *210*, 12–19. [[CrossRef](#)]
17. Meghwal, A.; Anupam, A.; Murty, B.S.; Berndt, C.S.; Kottada, R.S.; Ang, A.S.M. Thermal spray high-entropy alloy coatings: A review. *J. Therm. Spray. Tech.* **2020**, 1–37. [[CrossRef](#)]
18. Oksa, M.; Turunen, E.; Suhonen, T.; Varis, T.; Hannula, S.-P. Optimization and characterization of high velocity oxy-fuel sprayed coatings: Techniques, materials, and applications. *Coatings* **2011**, *1*, 17–52. [[CrossRef](#)]
19. Adachi, S.; Ueda, N. Formation of expanded austenite on a cold-sprayed AISI 316L coating by low-temperature plasma nitriding. *J. Therm. Spray. Tech.* **2015**, *24*, 1399–1407. [[CrossRef](#)]
20. Lindner, T.; Kutschmann, P.; Löbel, M.; Lampke, T. Hardening of HVOF-sprayed austenitic stainless-steel coatings by gas nitriding. *Coatings* **2018**, *8*, 348. [[CrossRef](#)]

21. ASTM International. *ASTM Standard G99-17 Standard Test Method for Wear Testing with a Pin-On-Disk Apparatus*; ASTM International: West Conshohocken, PA, USA, 2017.
22. ASTM International. *ASTM Standard G133-05 Standard Test Method for Linearly Reciprocating Ball-On-Flat Sliding Wear*; ASTM International: West Conshohocken, PA, USA, 2016.
23. ASTM International. *ASTM Standard G171-03 Standard Test Method for Scratch Hardness of Materials Using a Diamond Stylus*; ASTM International: West Conshohocken, PA, USA, 2017.
24. Petrova, R.S.; Suwattananont, N.; Samardzic, V. The effect of boronizing on metallic alloys for automotive applications. *J. Mater. Eng. Perform.* **2008**, *17*, 340–345. [[CrossRef](#)]



© 2020 by the authors. Licensee MDPI, Basel, Switzerland. This article is an open access article distributed under the terms and conditions of the Creative Commons Attribution (CC BY) license (<http://creativecommons.org/licenses/by/4.0/>).